Available online at www.sciencedirect.com
ScienceDirect
Polymer 48 (2007) 2980–2987
polymer
www.elsevier.com/locate/polymer

Spherulite morphology and crystallization behavior of poly(trimethylene terephthalate)/poly(ether imide) blends

Jong Kwan Lee, Mi Ju Choi, Jeong Eun Im, Dong Jun Hwang, Kwang Hee Lee*

Department of Polymer Science and Engineering, Inha University, 253, Yonghyun-dong, Nam-gu, Incheon 402-751, Republic of Korea

Received 18 October 2006; received in revised form 1 February 2007; accepted 25 February 2007
Available online 7 March 2007

Abstract

The spherulite morphology and crystallization behavior of poly(trimethylene terephthalate) (PTT)/poly(ether imide) (PEI) blends were investigated with optical microscopy (OM), small-angle light scattering (SALS), and small-angle X-ray scattering (SAXS). Thermal analysis showed that PTT and PEI were miscible in the melt over the entire composition range. The addition of PEI depressed the overall crystallization rate of PTT and affected the texture of spherulites but did not alter the mechanism of crystal growth. When a 50/50 blend was melt-crystallized at 180 °C, the highly birefringent spherulite appeared at the early stage of crystallization ($t < 20$ min). After longer times, the spherulite of a second form was developed, which exhibited lower birefringence. The SALS results suggested that the observed birefringence change along the radial direction of the spherulite was mainly due to an increase in the orientation fluctuation of the growing crystals as the radius of spherulite increased. The lamellar morphological parameters were evaluated by a one-dimensional correlation function analysis. The amorphous layer thickness showed little dependence on the PEI concentration, indicating that the noncrystallizable PEI component resided primarily in the interfibrillar regions of the growing spherulites.

Keywords: Spherulite morphology; Crystallization behavior; PTT

1. Introduction

The analysis of the morphology of crystalline polymer blends has gained significant momentum over the years. Much attention has been focused on the variety of microstructures that result from the crystallization of semicrystalline/amorphous blends [1–4]. One of the important considerations in this area is the location of the amorphous polymeric diluent in the microstructure. The diluent molecules can reside in interspherulitic regions, interfibrillar regions (i.e. between the lamellar stacks), interlamellar regions, or some combination of these, yielding different microstructures. The disposition of the polymeric diluent during crystallization depends on two factors: the first is the diffusion of the diluent molecules and the second is the growth rate of the crystal phase [1,3]. If the diffusion is slow and/or the growth rate is fast, the diluent molecules can be trapped between the lamellar, resulting in an interlamellar morphology. When the diffusion is fast and/or the growth rate is slow, the diluent molecules can diffuse out of the lamellar stacks, resulting in an interfibrillar or interspherulitic morphology.

Poly(trimethylene terephthalate) (PTT) possesses good mechanical properties. However, the lower glass transition temperature ($T_g = 44$ °C) of PTT is a disadvantage in some applications. Poly(ether imide) (PEI) is a high-performance engineering plastic with a T_g of approximately 215 °C. However, due to its amorphous nature PEI is poor for chemical resistance. Therefore, it is expected that the blending of PTT and PEI offers a viable means of combining the complementary properties of both polymers [5]. In this paper, the morphology development and crystallization behavior of a melt-mixed crystalline/amorphous system consisting of PTT and PEI are reported. The miscibility was studied with differential scanning calorimetry (DSC) and a dynamic mechanical thermal

* Corresponding author. Tel.: +82 32 862 9507; fax: +82 32 865 5178.
E-mail address: polylee@inha.ac.kr (K.H. Lee).

0032-3861/$ - see front matter © 2007 Elsevier Ltd. All rights reserved.
doi:10.1016/j.polymer.2007.02.070

analyzer (DMTA). The spherulitic morphology and the crystallization behavior were probed using optical microscopy (OM), small-angle light scattering (SALS) and small-angle X-ray scattering (SAXS).

2. Experimental

2.1. Materials and sample preparation

PTT with the molecular weight of ~23,000 was obtained from SKC Co., Korea. PEI was supplied by General Electric (GE, Ultem 1000) and its number- and weight-average molecular weights were $\overline{M_n} = 12,000$ and $\overline{M_w} = 30,000$, respectively. After being dried in a vacuum oven at 150 °C for 24 h, PTT and PEI were melt-mixed at 280 °C on a 30-mm co-rotating twin-screw extruder (Werner Pfleiderer) at 200 rpm. The extrudate was quenched in ice water and was then chopped into pellets. The blend compositions are indicated in ratios of weight percent, the first numeral referring to PTT throughout this paper.

Samples for the DMTA study were prepared by compression molding. The pellets were compression-molded between metal plates at 280 °C for 5 min followed by quenching in ice water to obtain an amorphous specimen of ~1 mm thick.

2.2. Thermal analysis

The thermal properties of the melt-quenched samples were investigated with a Perkin–Elmer DSC-7 differential scanning calorimetry (DSC). The samples were heated to 300 °C at a rate of 10 °C/min in a nitrogen atmosphere. Dynamic mechanical measurements were performed with a Polymer Laboratories MKIII dynamic mechanical thermal analyzer (DMTA). DMTA was operated in the dual-cantilever banding mode at a frequency of 1 Hz and a heating rate of 3 °C/min from 25 to 250 °C.

2.3. SALS and OM

A thin-film specimen (ca. 15 μm thick) was prepared by melt-pressing the pellets between two cover glasses. After the specimen was held at 280 °C for 5 min, it was rapidly transferred onto a hot-stage set at the desired crystallization temperature in a light scattering photometer equipped with a charged-coupled device camera, and the supermolecular structures were then examined. A polarized He–Ne gas laser with a 632.8 nm wavelength was applied to the specimen. H_v geometry was used, in which the optical axis of the analyzer was set perpendicular to that of the polarizer. The spherulitic morphology of the specimens was also observed with OM.

2.4. SAXS

All SAXS measurements were performed at room temperature. The X-ray beam was from synchrotron radiation, beam line 4C1 at the Pohang Light Source, Korea. The storage ring was operated at an energy level of 2 GeV. The SAXS employs point focusing optics with a Si double crystal monochromator followed by a bent cylindrical mirror. The incident beam intensity of 0.149 nm wavelength was monitored by an ionization chamber for the correction of a minor decrease of the primary beam intensity during the measurement. The scattering intensity by thermal fluctuations was subtracted from the SAXS profile $I(q)$ by evaluating the slope of a $I(q)\cdot q^4$ *vs.* q^4 plot at wide scattering vector q, where q is $(4\pi/\lambda)\sin(\theta/2)$, and λ and θ are the wavelength and scattering angle, respectively [6]. A correction for the smearing effect by the finite cross-section of the incident beam was not necessary for the optics of SAXS with point focusing.

3. Results and discussion

The glass transition temperature (T_g) may provide useful information on blend miscibility [7]. For an immiscible blend, two T_gs generally appear on a DSC scan, whereas for miscible blends or copolymers, only one T_g is observed. Fig. 1 shows DSC traces for quenched PTT, PEI, and PTT/PEI blends at a heating rate of 10 °C/min. For all compositions, only one T_g, which is marked by the arrow in the figure, is observed. T_g rises monotonically as the PEI content in the blend increases, suggesting that the blends are completely miscible. Furthermore, both the cold crystallization temperature and the width of the exotherm increase as the PEI content increases. These results imply that the presence of PEI retards PTT crystallization, which is normally expected from a miscible polymer pair. By increasing the PEI content in the blend, the melting temperature gradually decreases from 229 to 226 °C. No trace of melting endotherm can be observed for the blend containing less than 50% PTT, indicating that the crystallization rate significantly decreases as the PEI content in the blend increases. A prior study [5] gave a similar result.

Dynamic mechanical measurements also provide supplementary evidence for the miscibility of the blend. The temperature dependence of the loss tangent, $\tan\delta$ of the

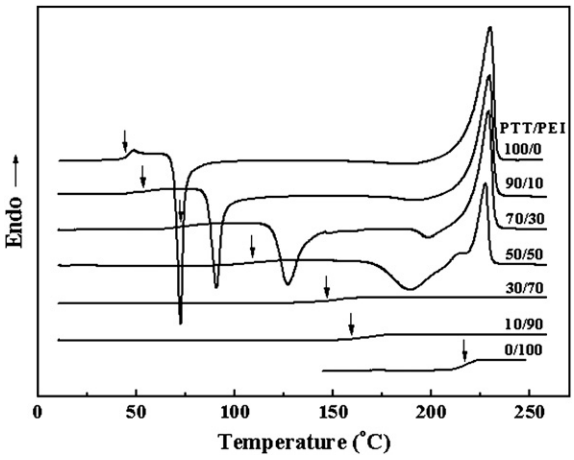

Fig. 1. DSC thermograms of the melt-quenched samples. The blend compositions are indicated in the figure.

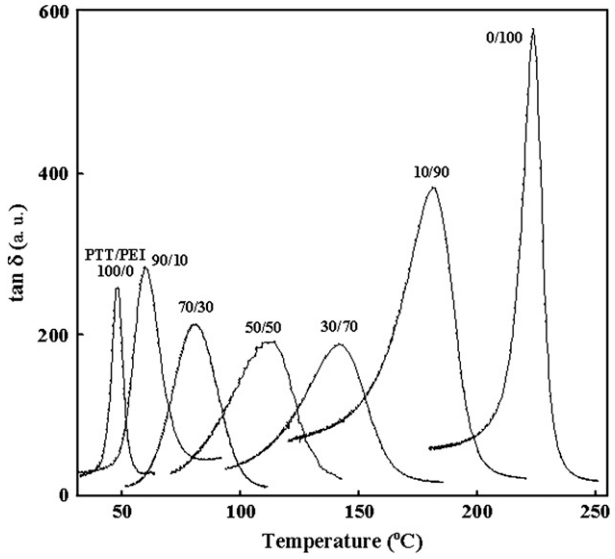

Fig. 2. Temperature dependence of the loss tangent (tan δ) of the melt-quenched samples.

melt-quenched samples is plotted in Fig. 2. The samples show a single glass transition, the temperature of which shifts to higher temperatures as the PEI content increases. As can be seen, in all cases the glass transition width is wider for the blends than it is for the pure PTT and PEI. It is important to note that the broad range of the tan δ peaks depends on the degree of segmental mixing on a molecular scale. The observation of the wide breadth of the tan δ peak for the blends suggests that small-scale compositional fluctuations still reside in the amorphous state, although the PTT/PEI blends are optically transparent.

The spherulitic morphology of the blends was examined at various crystallization temperatures between 150 and 200 °C. The greatest morphological change was found when the samples were crystallized at 175–185 °C. Fig. 3 shows polarized optical micrographs of the samples crystallized from the melt at various temperatures. The crystallization of PTT, which amounts to a transition from a fully amorphous to a amorphous/crystalline state, proceeds through the free growth of the spherulites from a homogeneous melt. All the spherulites display the characteristic ''Maltese Cross'' extinction pattern, and several also exhibit regular concentric bands. The Maltese Cross arises from the coincidence of the principle axis of the crystal with the extinction direction of the polarizer or analyzer. It can easily be demonstrated that the chains are arranged circumferentially within the spherulites. The regular concentric bands arise from a regular twist in the radiating lamellae. The mechanisms of lamellar twisting within spherulite are referred to two models. They are interlamellar and intralamellar origins. For interlamellar origin, equally spaced screw dislocations along the radial growth direction of the lamellae are formed so as to give rise to the twisting of molecular stems at the lamellar level. The model was originally

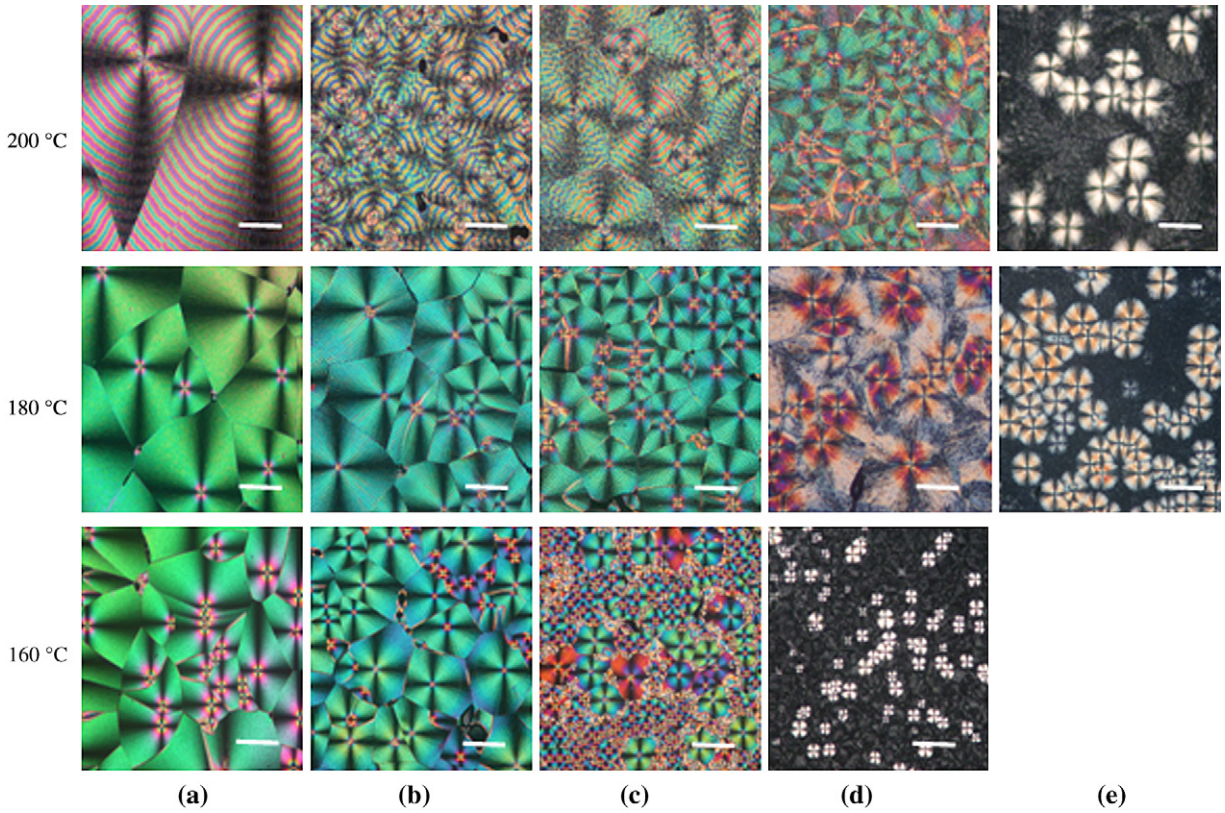

Fig. 3. Optical micrographs (equivalent magnification, bar = 50 μm) of the spherulitic morphology of the PTT/PEI blends crystallized at the temperatures indicated in the figure. The blend compositions: (a) 100/0; (b) 90/10; (c) 70/30; (d) 50/50; (e) 30/70.

proposed by Schultz and Kinloch [8] and then modified by Bassett and co-workers in detail [9–11]. For intralamellar origin, regularly twisted molecular stems are cooperatively accommodated in continuously twisted helical lamellae without the presence of screw dislocations. The twisting is attributed mainly to the influence of the surface stresses resulting from the asymmetry of lamellar geometry. The model was initially proposed by Keller [12] and has been developed intensively by Keith and Padden [13–15]. Recently, a detailed investigation on the formation of the banded spherulites of PTT was achieved by Ho et al. [16]. They suggested that the lamellar twisting was attributed to the tilted chain stems which were nonorthogonal to fold surface. The nonorthogonal geometry resulted from the growth of PTT lamellae with triclinic structure where internal stress was gradually accumulated so as to drive the crystal twist along the radial direction of spherulite. In other words, the twisting of PTT lamellae was attributed to an intralamellar origin to the lamellar geometry. However, it should be noted that many polymeric materials appear the morphology of banded spherulites and different mechanisms have been proposed to interpret various systems. In the pure PTT samples crystallized at 160 and 180 °C, the bands are spaced very tightly and are not resolved at the current magnification. It is usually found that the band spacing increases with the crystallization temperature but decreases with the addition of noncrystallizing diluents [17–19]. Thus, the observed increase in the band spacing with the addition of PEI for the samples crystallized at 180 °C as shown in Fig. 4 is contrary to common findings. The reason for this is not entirely clear. It was observed that the spherulites become progressively smaller as the PEI content increases, indicative of an increase in nucleation density due to blending. Up to high PEI content levels, the PTT spherulites remain relatively space filling, although nonbirefringent regions develop at the spherulitic boundaries in PEI-rich blends. The fact that the PTT phase is relatively space filling even with a high PEI content indicates that the noncrystallizable PEI component, which is rejected in the crystallization process, is incorporated into the interlamellar and/or interfibrillar regions of the spherulites. One of the interesting features in Fig. 3 is the change in the interference colors. Most of the spherulites show vivid interference colors without a sensitive tint plate, as the birefringence of the PTT spherulite is extremely large [20]. As the PEI content increases, the interference color of the spherulites changes with a sequence of green–red–yellow. The appearance of this color sequence is associated with a change in the birefringence in the spherulites. The birefringence in the spherulite Δn is described by:

$$\Delta n = \Delta n^0 \phi f \tag{1}$$

where Δn^0 is the intrinsic birefringence of crystallite (Δn^0 of PTT is 0.236 [21], which is similar to that of PET and other general polymers); ϕ is the crystallinity within the spherulite, and f is an orientation function describing the orientation of the crystals with respect to the radius of the spherulite. Thus, the change in the interference color of the spherulites suggests that the crystallinity within a spherulite and/or the degree of the orientation of the crystals can be decreased with an addition of the noncrystallizing PEI component. Another interesting feature in the figure is that less-ordered interference colors are observed at the center of the spherulites. This observation is consistent with the fact that a supermolecular structure with a low crystallinity and a low degree of orientation correlations of the constituent crystals is obtained at the initial stage of crystallization [22].

Another phenomenon worth mentioning is the change in the interference colors along the radial direction of the spherulite. Fig. 5 shows the polarized optical micrographs and the corresponding SALS H_v patterns of the 50/50 blend crystallized at 180 °C for various time intervals. The highly birefringent spherulite is observed at the early stage of crystallization ($t < 20$ min). After that, a spherulite of a second form is developed, which exhibits a lower birefringence and appears to be less compact. This observation indicates that during the later stage of crystallization the anisotropy of the growing crystal aggregate is low, suggesting a low crystallinity within the spherulite and/or a low degree of orientational correlations of the constituent crystals. At the later stage of crystallization ($t = 60$ min), the formation of new secondary crystallites and the perfection of existing crystals appear to take place within the spherulite. This is accompanied by a change in the birefringent appearance of the spherulite, which was observed to become brighter and exhibits a more pronounced interference color.

The radial growth rate of the spherulite was determined by monitoring the spherulite radius R as a function of time during isothermal crystallization in the hot-stage of a polarizing microscope. For the 50/50 blend crystallized at 180 °C, R was found to increase linearly in time up to the point of impingement, indicating a constant growth rate throughout the crystallization process (Fig. 6). The linearity of R implies that PEI molecules that are rejected from the growing PTT crystals, do not accumulate at the spherulite boundary, but rather become trapped within the interlamellar and/or

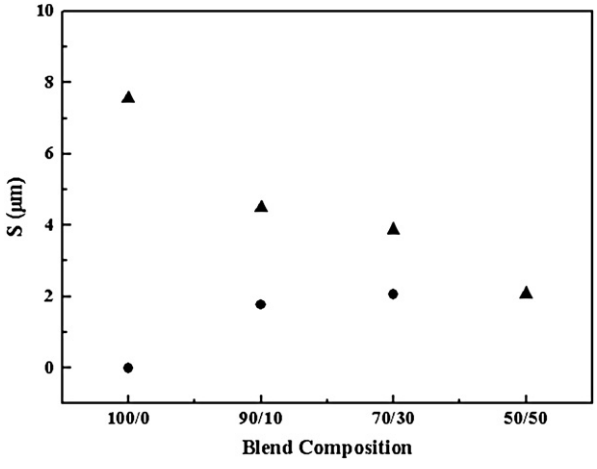

Fig. 4. Dependence of band spacing S on the blend compositions. The crystallization temperatures are: (●) 180 °C; (▲) 200 °C.

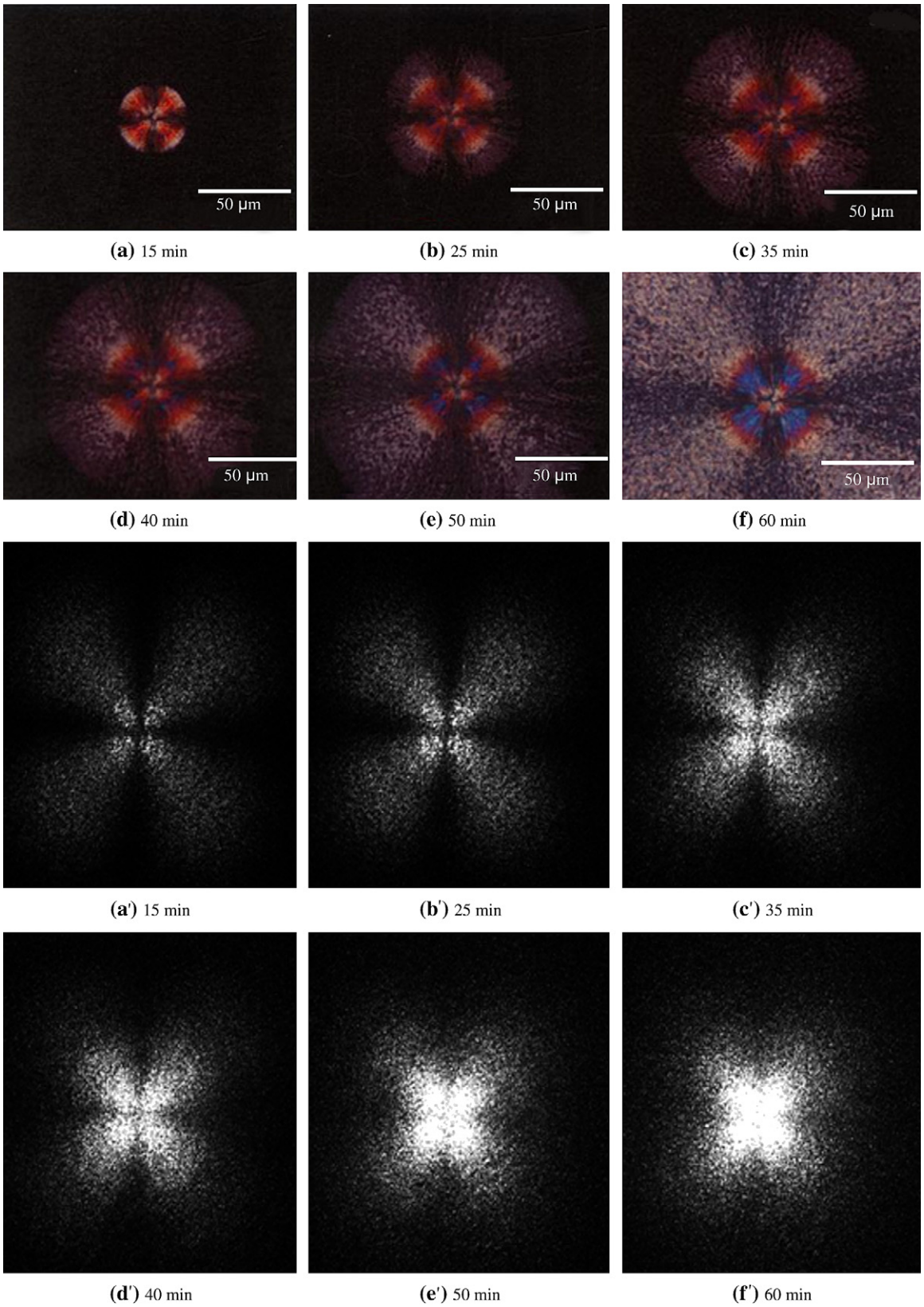

Fig. 5. Optical micrographs of the spherulitic morphology of the 50/50 blend crystallized at 180 °C for various time intervals and the corresponding SALS H_v patterns.

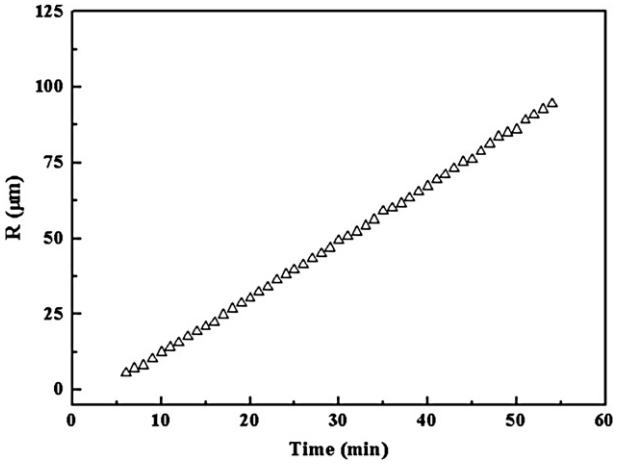

Fig. 6. Plot of the spherulite radius R as a function of the crystallization time.

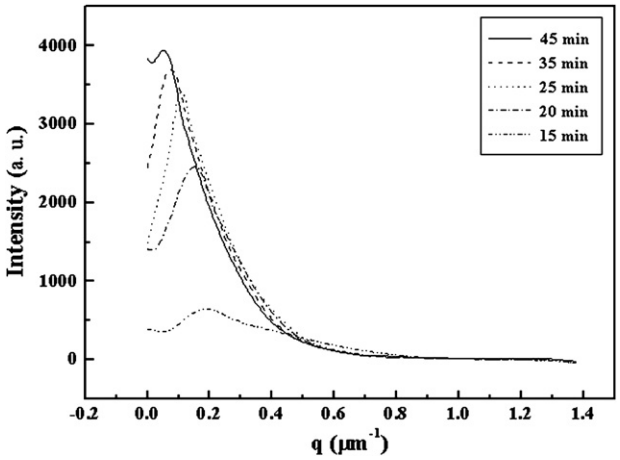

Fig. 7. Time evolution of the one-dimensional H_v scattering profiles at an azimuthal angle of 45° in the scattering patterns for the 50/50 blend crystallized at 180 °C.

interfibrillar regions of the growing spherulite [19]. It should be mentioned that the crystallinity within the spherulite remains constant during the isothermal crystallization if there is no change in the concentration of crystallizable elements at the crystal growth front [23,24]. It is therefore reasonable to assume that the observed birefringence spectrum is mainly caused by a change of the lamellar ordering along the radial direction of the spherulite.

The H_v scattering pattern is concerned with the arrangement of individual lamellar crystallites into a large scale of organization. Stein and Chu [25] suggested by a model calculation of the scattering patterns that lower orders of organization result in a broad H_v scattering pattern, i.e. as the disorder of lamellar orientation increases, the azimuthal dependence of the scattering pattern decreases. The orientation fluctuation of the lamellar crystals within a spherulite can be quantitatively described by introducing the disorder parameter ξ. Yoon and Stein [26] provided a calibration curve relating the parameter ξ to the ratio of intensity at $w = 4$ to that at $w = 15$, where w is a reduced angle parameter defined as:

$$w = (2\pi/\lambda)R \sin\theta \tag{2}$$

$$\xi = I(w = 4)/I(w = 15) \tag{3}$$

Fig. 7 shows the time evolution of one-dimensional H_v scattering profiles at an azimuthal angle of 45° in the scattering patterns for a 50/50 blend crystallized at 180 °C. The profiles have a maximum at a scattering angle of θ_m. The θ_m is related to the R [27]:

$$4.09 = 4\pi(R/\lambda)\sin(\theta_m/2) \tag{4}$$

Therefore, the shift of the peak positions to a lower value suggests that the size of the spherulite increases as the crystallization time increases. Fig. 8 shows the time dependence of the ξ obtained from Fig. 7. The calculated values of ξ remarkably decrease during the early stage of crystallization, which is consistent with other experimental observations in the literature [22,28]. An interesting feature is that the ξ increases during the later stage of crystallization, suggesting that the spherulitic structure significantly deteriorates as the radius of the spherulite increases. This result is in good agreement with microscopic observation, as shown in Fig. 5. The disordering of the spherulite observed at the later stage of crystallization can be interpreted by considering the dendritic and densely branched internal structure. A number of lamellae will extend from the center of a spherulite all the way to the outer boundary. They form the basic skeleton for the entire spherulite. When a crystal branches at the inner part of the spherulite, the branching crystal can be aligned nearly side by side with the mother crystals as the skeleton lamellae are closely packed. As the radius of the spherulite increases, the gaps between the radiating lamellae will increase. Consequently, the branching crystal may tend to splay away from the mother crystal, leading to a spherulitic structure of decreasing order at the outer part of the spherulite. However, further experimental investigations, e.g. transmission electron microscopy (TEM), will be needed to clarify this.

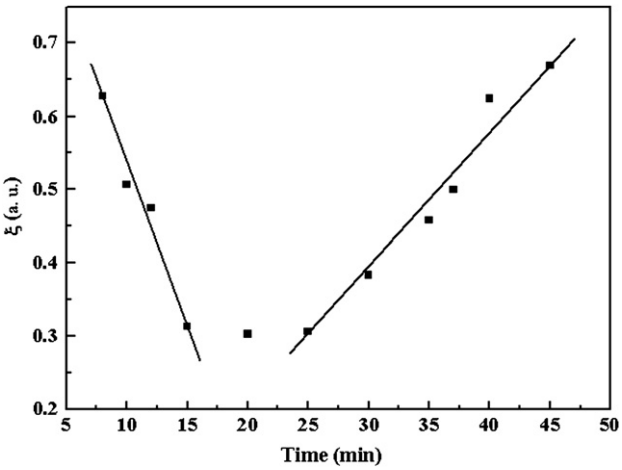

Fig. 8. Time dependence of the disorder parameter ξ.

Fig. 9 shows typical time-resolved SAXS profiles of a 50/50 blend crystallized at 180 °C. It is observable that the scattering peak begins to appear near 20 min and increases to a plateau value at approximately 100 min. The peak position slightly shifts to a larger scattering vector as the time increases, which may be attributed to the secondary crystallization process. It is believed that the secondary crystals possess a thinner lamellar thickness and a defective crystal structure due to the chain ends, low molar-mass species, and lower entropy restraints in the amorphous regions imposed by the primary crystals. It is interesting to note that what is known as the secondary crystallization stage is normally considered to occur at longer times after the space filling of the spherulites, while physical justification for the growth of secondary stacks of lamellae during the primary crystallization process was given some years ago [3,29], and has also been modeled more recently [30].

The SAXS data were analyzed via the modified correlation function method [31]. This method is based on the use of two alternative expressions to estimate the Porod approximation. From this method, it is possible to calculate the long period (L) and the thicknesses of the constituent phases (crystalline and amorphous) (l_c and l_a). The effect of the blend compositions on the morphological changes at the lamellar level is represented in Fig. 10. The values of l_c slightly increase as the PEI content increases. This behavior can be explained simply through thermodynamic considerations. As can be seen in Fig. 1, the melting point of the blends decreases as the PEI content increases, due to the diluent effect of the noncrystallizable species. A lower melting point in the blends causes a lower degree of undercooling; therefore, it is expected that l_c will increase as the PEI content increases at a given crystallization temperature as a result of the corresponding decrease in the degree of undercooling. It is worth noting that the amorphous layer thickness is relatively independent of the blend compositions. All blends exhibit approximately the same l_a. In view of the fact that an interlamellar incorporation should result in a monotonic increase of the amorphous layer thickness with the PEI content, the constant value of l_a implies that PEI molecules are expelled out of the interlamellar regions and consequently reside in the interfibrillar regions. This is reasonable when one considers the observations of the space-filling spherulitic texture and constant growth rate, as shown in Figs. 3 and 6.

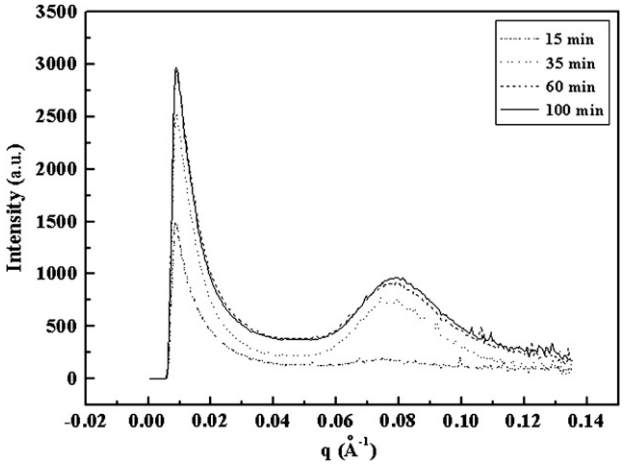

Fig. 9. Time-resolved SAXS profiles of the 50/50 blend crystallized at 180 °C. The crystallization times are indicated in the figure.

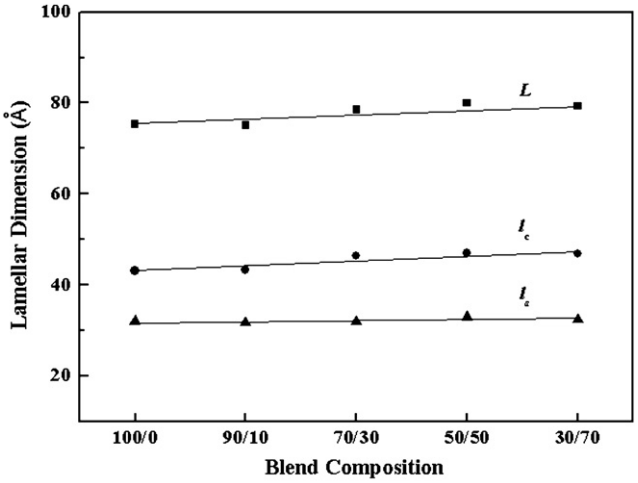

Fig. 10. Plots of the lamellar dimensions (L, l_c, and l_a) against the blend compositions. The samples were crystallized at 180 °C.

4. Conclusions

In this study, the morphological changes and crystallization behavior of PTT/PEI blends were examined. The spherulitic morphology of PTT crystals was largely affected by the addition of PEI. For a 50/50 blend sample crystallized at 180 °C, a change in the birefringence along the radial direction of spherulite was observed. A SALS analysis suggested that the observed birefringence change was mainly due to an increase in the orientation fluctuation of the growing crystals as the radius of the spherulite increased. The amorphous layer thickness showed little dependence on the PEI concentration. The constant value of l_a suggested that the diffusion rate of PEI may be faster than the growth rate of crystals, with most of PEI molecules escaping from the PTT lamellar stacks. As a result, the noncrystallizable PEI component was primarily incorporated into the interfibrillar regions of the growing spherulites.

Acknowledgments

This research was supported by an Inha University Research Grant. Synchrotron small-angle X-ray scattering experiments were performed at the Pohang Light Source (4C1 beam line) in Korea.

References

[1] Talibuddin S, Wu L, Runt J, Lin JS. Macromolecules 1996;29(23): 7527–35.
[2] Chen HL, Li LJ, Lin TL. Macromolecules 1998;31(7):2255–64.

[3] Yeh F, Hsiao BS, Chu B, Sauer BB, Flexman EA. J Polym Sci Polym Phys Ed 1999;37(21):3115–22.
[4] Dreezen G, Mischenko N, Koch MHJ, Reynaers H, Groeninckx G. Macromolecules 1999;32(12):4015–22.
[5] Huang JM, Chang FC. J Appl Polym Sci 2002;84(4):850–6.
[6] Koberstein J, Morra B, Stein RS. J Appl Crystallogr 1980;13:34.
[7] Porter RS, Wang LH. Polymer 1992;33(10):2019–30.
[8] Schultz JM, Kinloch DR. Polymer 1969;10:271–8.
[9] Bassett DC, Hodge AM. Polymer 1978;19(4):469–72.
[10] Bassett DC, Vaughan AS. Polymer 1985;26(5):717–25.
[11] Bassett DC, Olley RH, AlRaheil IAM. Polymer 1988;29(9):1539–43.
[12] Keller A. J Polym Sci 1955;17(84):291–308.
[13] Keith HD, Padden Jr FJ. J Polym Sci 1959;39(135):101–22.
[14] Keith HD, Padden Jr FJ. J Polym Sci 1959;39(135):123–38.
[15] Keith HD, Padden Jr FJ. Polymer 1984;25(1):28–42.
[16] Ho RM, Ke KZ, Chen M. Macromolecules 2000;33(20):7529–37.
[17] Keith HD, Padden Jr FJ, Russell TP. Macromolecules 1989;22(2):666–75.
[18] Pizzoli M, Scandola M, Cerrorulli G. Macromolecules 1994;27(17):4755–61.
[19] Penning JP, Manley RSJ. Macromolecules 1996;29(1):84–90.
[20] Yun JH, Kuboyama K, Ougizawa T. Polymer 2006;47(5):1715–21.
[21] Bae JH, Kim YH, Kim KJ. Fifth ATC, Kyoto, Japan; 1999. p. 973.
[22] Lee CH, Saito H, Inoue T. Macromolecules 1993;26(24):6566–9.
[23] Wang ZG, Phillips RA, Hsiao BS. J Polym Sci Polym Phys Ed 2000;38(19):2580–90.
[24] Akpalu Y, Keilhorn L, Hsiao BS, Stein RS, Russell TP, van Egmond J, et al. Macromolecules 1999;32(3):765–70.
[25] Stein RS, Chu W. J Polym Sci A-2 1970;8(7):1137–57.
[26] Yoon DY, Stein RS. J Polym Sci Polym Phys Ed 1974;12(4):763–84.
[27] Stein RS, Rhodes MB. J Appl Phys 1960;31(11):1873–84.
[28] Lee CH, Saito H, Inoue T. Macromolecules 1995;28(24):8096–101.
[29] Hillier IH. J Polym Sci Part A Gen Pap 1965;3(9):3067–78.
[30] Hsiao BS, Chang IY, Sauez BB. Polymer 1991;32(15):2799–805.
[31] Hsiao BS, Verma RK. J Synchrotron Radiat 1998;5(1):23–9.